De Novo Design of Star-Shaped Glycoligands with Synthetic Polymer Structurestoward an Influenza Hemagglutinin Inhibitor

Nagao, Masanori
Department of Chemical Engineering, Kyushu University

Yamaguchi, Ai
Department of Biosciences and Informatics, Keio University

Matsubara, Teruhiko
Department of Biosciences and Informatics, Keio University

Hoshino, Yu
Department of Chemical Engineering, Kyushu University

他

出版情報：Biomacromolecules. 23 (3), pp.1232-1241, 2022-03-14. American Chemical Society
バージョン：
権利関係：

De Novo Design of Star-Shaped Glycoligands with Synthetic Polymer Structures Toward an Influenza Hemagglutinin Inhibitor

Masanori Nagao,[*a] *Ai Yamaguchi,*[b] *Teruhiko Matsubara,*[b] *Yu Hoshino,*[a] *Toshinori Sato*[b] *and Yoshiko Miura**[a]

AUTHOR ADDRESS.

[a] Department of Chemical Engineering, Kyushu University, 744 Motooka Nishi-ku, Fukuoka 819-0395, Japan.

[b] Department of Biosciences and Informatics, Keio University, 3-14-1 Hiyoshi, Kohoku-ku, Yokohama, Kanagawa 223-8522, Japan.

KEYWORDS. Synthetic polymers, controlled polymerization, Gaussian models, carbohydrates, influenza virus, multivalent interaction.

ABSTRACT: Synthetic polymers with well-defined structures allow the development of nanomaterials with additional functions beyond biopolymers. Herein, we demonstrate *de novo* design of star-shaped glycoligands to interact with hemagglutinin (HA) using well-defined synthetic polymers, with the aim of developing an effective inhibitor for the influenza virus. Prior to the synthesis, the length of the star polymer chains was predicted using the Gaussian model of synthetic polymers, and the degree of polymerization required to achieve multivalent binding to three carbohydrate recognition domains (CRDs) of HA was estimated. The star polymer with the predicted degree of polymerization was synthesized by reversible addition-fragmentation chain transfer (RAFT) polymerization, and 6'-sialyllactose was conjugated as the glycoepitope for HA. The designed glycoligand exhibited the strongest interaction with HA as a result of the multivalent binding. This finding demonstrated that the biological function of the synthetic polymer could be controlled by precisely defining the polymer structures.

Introduction

In the field of nanoscience, one key objective is to control molecular functions using molecular structures. DNA and proteins (peptides) are natural biofunctional nanomaterials, and their well-defined structures allow *de novo* design of the functions (e.g., self-assembly and molecular recognition).[1–4] Synthetic polymers are a class of nanomaterials with advantages such as chemical stability, easy synthesis, and the availability of a versatile range of appropriate monomers. The industrial use of synthetic polymers is mainly for bulk materials; however, individual synthetic polymer molecules can have sizes in the same range as the biomacromolecules mentioned above. In contrast to the homogeneous structures of DNA and peptides, the structures of synthetic polymers are heterogeneous in terms of their molecular weight, monomer sequence, and conformation. As the versatility of the synthetic monomers allows synthetic polymers to have additional functions beyond those of biomacromolecules, improving the precision of the polymer structures is expected to lead to the development of novel nanomaterials.[5,6]

Controlled polymerization techniques have been developed to reduce the heterogeneity of synthetic polymers.[7] Polymerization techniques including living radical polymerization have provided synthetic polymers with well-defined primary structures in terms of molecular weight and monomer sequence.[8,9] Recently, polymerization techniques allowing further polymer structure precision have been developed. The single unit monomer insertion technique enables the addition of monomers one-by-one,[10,11] and iterative exponential growth polymerization produces polymers by repeating the coupling reaction between the well-defined segments.[12,13] Synthetic polymers with discrete structures can be used as storage of information[14,15] or as

abiotic ligands,[16] demonstrating that the homogeneity enhances the potential of synthetic polymers as nanomaterials.

Intermolecular interaction is one of the functions of biomolecules. The carbohydrate–protein interaction is an important interaction for biological phenomena, as is the protein–protein interaction.[17] Glycoconjugates on cells bind to the corresponding proteins (lectins) and induce physiological phenomena such as immune responses and pathogen infections.[18] Although the monomeric interaction between a terminal carbohydrate and a carbohydrate recognition domain (CRD) of a lectin is weak (binding constant $K_a = 10^{-3}$ M), multivalent binding between the carbohydrates and CRDs of a lectin enhances the total interaction ($K_a > 10^{-6}$ M).[19] This enhancement is ubiquitous in biological systems, and in particular, is known as the cluster glycoside effect in glycoscience.[20] Synthetic glycoligands with a high affinity for the target lectins through the cluster glycoside effect are effective inhibitors against pathogens.[21–24] To achieve the cluster glycoside effect with a synthetic glycoligand for a target lectin, the spatial arrangement of the glycoepitopes of the ligand must be comparable to the distance between the CRDs of the target lectin.[25–27] Synthetic polymers with controlled structures are expected to enable the precise design of glycoligands, leading to biofunctional nanomaterials.[28]

The influenza virus is an important target in biomedical science owing to the threat of pandemic.[29] Hemagglutinin (HA) is a membrane protein of the virus and has a homotrimeric structure. Each subunit has one CRD (three CRDs per HA molecule), and the CRDs are located at the vertices of the triangle formed on the HA surface.[30] The virus enters a cell through the multivalent interaction between HA molecules and sialyl oligosaccharides on the cell surface. Thus, glycoligands that bind to HA are expected to inhibit viral infection. Ebara and co-workers reported the design of glycoligands based on three-way junction DNA,[31] and Meyer and co-

workers reported the *in silico* design of glycoligands using peptide linkers.[32] In these reports, the glycoligands were trivalent and were designed to have appropriate linker length to allow multivalent binding to the three CRDs of HA. Our group reported the synthesis of well-defined glycopolymers as polymer ligands against the influenza virus.[33–35] The structural factors such as glycoepitope density, polymer length, and polymer topology, were controlled by living radical polymerization to realize multivalent binding to HA. However, unlike DNA and peptides, *de novo* design of glycoligands using synthetic polymers based on prior prediction of the appropriate polymer structure against the target biomolecule has not been reported. For synthetic polymers to be applied as useful nanomaterials, tailor-made synthesis of the synthetic polymers with the precision possible for DNA and peptides, must be achieved.

Herein, we describe the *de novo* design of star-shaped glycoligands using synthetic polymers, to control interactions with HA. The star-shaped glycoligand was designed with 6'-sialyllactose (6'-SALac) at the terminals of the polymer arms as glycoepitopes (one 6'-SALac per arm). Prior to the synthesis of the star polymers, the degree of polymerization required to achieve multivalent binding to the three CRDs of HA was estimated using classical theoretical polymer models. A well-defined star polymer with the predicted degree of polymerization was then synthesized as a scaffold for the glycoepitopes by reversible addition-fragmentation chain transfer (RAFT) polymerization. *N*,*N*-Dimethylacrylamide (DMA) was used as the hydrophilic monomer owing to both of the inertness to biomolecular recognition and of the polymerization property suitable for secondary R-group of the trifunctional RAFT agent. The interaction of the glycoligand with the influenza virus was evaluated, and the validity of the molecular prediction is discussed.

Experimental Section

Materials. Triethylamine (TEA, 99%), trimethylolethane (98%), 1-ethyl-3-(3-dimethyl aminopropyl)carbodiimide hydrochloride (EDC·HCl, 98%), 4-methoxyphenol (99%), acryloyl chloride (95%), propargyl alcohol (98%), lithium bromide (LiBr, 99%) and *N*,*N*-dimethylacrylamide (DMA, 99%) were purchased from Tokyo Chemical Industry (Tokyo, Japan). 4-Dimethylaminopyridine (DMAP, 99%), 2,2'-azobis[2-(2-imidazolin-2-yl)propane] dihydrochloride (AIPD, 98%) and formic acid (99%) were purchased from Wako Pure Chemical Industries (Osaka, Japan). Diethylether (Et_2O), *N*,*N*-dimethylformamide (DMF), copper(II) sulfate ($CuSO_4$, 97.5%), and sodium L-ascorbate (98%) were purchased from Kanto Chemical (Tokyo, Japan). Acetonitrile (MeCN) and fetuin from fetal bovine serum were purchased from Sigma Aldrich (St. Louis, USA). Blood cell suspension from a chicken was purchased from Nippon Bio-test Laboratory Inc (Saitama, Japan). 2-{[(Butylsulfanyl)carbonothioyl]sulfanyl}-propanoic acid (BTPA),[36] 6'-sialyllactose azide (6'-SALac azide),[37] and trifunctional RAFT agent[35] were prepared according to previous papers. Commercial monomers including the radical inhibitor were purified by passing through an alumina column prior to use.

Characterizations. Proton and carbon nuclear resonance (^{1}H NMR and ^{13}C NMR) spectra were recorded on a JEOL-ECP400 spectrometer (JEOL, Tokyo, Japan) using $CDCl_3$ or D_2O as a solvent. Size exclusion chromatography (SEC) analyses with water solvent was performed on a JASCO DG-980-50 degasser equipped with a JASCO PU-980 pump (JASCO Co., Tokyo, Japan), a Shodex OH pak SB-G guard column, a Shodex OH pak SB-803 HQ column (Showa Denko, Tokyo, Japan), a JASCO RI-2031 Plus RI detector, and a Viscotek TDA (Malvern Instruments Ltd., Worcestershire U.K.). The analysis was performed at a flow rate of 0.5 mL/min by injecting 20 μL of a polymer solution (2 g/L) in 100 mM $NaNO_3$ aqueous solution. The SEC

system was calibrated using a pullulan standard (Shodex). All the samples were previously filtered through a 0.22 μm filter. SEC with organic solvent was performed on a HLC-8320 GPC Eco-SEC equipped with a TSKgel Super AW guard column and TSKgel Super AW (4000 and 2500) columns (TOSOH, Tokyo, Japan). The SEC analyses were performed at a flow rate of 0.5 mL/min by injecting 20 μL of a polymer solution (2 g/L) in DMF with 10 mM LiBr. The SEC system was calibrated with a polystyrene standard (Shodex). All the samples for SEC were previously filtered through a 0.45 μm filter. UV-vis spectra were recorded at 25 °C using an Agilent 8453 spectrophotometer (Agilent Technologies, Santa Clara, CA, USA). Dynamic light scattering (DLS) measurements were performed on a ZETASIZER NANO-ZS (Malvern, UK) by using a 1 mL disposable cell of a polymer solution (1 mg/mL) in the buffer solution. All the samples for DLS were previously filtered through a 0.22 μm filter. The water used in this research was purified using a Direct-Q Ultrapure Water System (Merck, Ltd, Darmstadt, Germany).

Synthesis of propargyl acrylate. To the mixture solution of propargyl alcohol (14.6 g, 260 mmol) and TEA (47.1 mL, 338 mmol) in Et_2O (120 mL), acryloyl chloride (25.2 mL, 312 mmol) in Et_2O (120 mL) was added dropwise at 0 °C. The mixture solution was stirred at room temperature overnight. The precipitation was removed by filtration, and the filtrate was purified by silica gel chromatography (EtOAc: hexane = 1: 4). The fraction was concentrated with a small amount of 4-methoxyphenol. The product was obtained as colourless oil (7.79 g, 27%).

^{1}H NMR (400 MHz, $CDCl_3$) δ in ppm: 6.48 (dd, J = 17.2 Hz, *trans* CH_2=CH, 1H), 6.15 (dd, J = 17.6 Hz, CH_2=CH, 1H), 5.89 (dd, J = 10.8 Hz, *cis* CH_2=CH, 1H), 4.76 (d, J = 2.4 Hz, -COOCH2-, 2H), 2.49 (t, J = 2.0, 2.8 Hz CH2-C≡CH, 1H).

^{13}C NMR (100 MHz, $CDCl_3$) δ in ppm: 165.4 (carbonyl), 132.1 (vinyl), 127.7 (vinyl), 75.1 (alkynyl), 52.2 (-CH2-ester).

Synthesis of bifunctional RAFT agent. To the solution of BTPA (794 mg, 3.33 mmol), trimethylolethane (200 mg, 1.66 mmol), and DMAP (49 mg, 0.4 mmol) in dry CH_2Cl_2 (30 mL), EDC·HCl (660 mg, 3.44 mmol) was added at 0 °C (the color changed to red from yellow). After being stirred for 10 min, the ice bath was removed. The solution was stirred at room temperature for 16 h. The progress of the reaction was confirmed on TLC (EtOAc: Hexane = 1: 4). The organic phase was washed with 1 wt% HCl (aq) (30 mL × 3), Milli-Q water (30 mL × 2), and dried with Na_2SO_4. The filtrate was concentrated under reduced pressure, and purified by column chromatography (EtOAc: Hexane = 1: 4, R_f = 0.25). The product was obtained as yellow oil (172 mg, 18%).

^{1}H NMR (400 MHz, $CDCl_3$) δ in ppm: 4.85 (q, 2H, ester–C**H**(CH_3)–S), 4.05 (m, 4H, CH_3–(C**H**$_2$–ester–)$_2$), 3.40 (s, 2H, HO–C**H**$_2$–), 3.35 (t, 4H, –S–C**H**$_2$–C_3H_7), 1.67 (quin, 4H, –SCH_2–C**H**$_2$–C_2H_5), 1.60 (d, 6H, ester–CH(C**H**$_3$)–S), 1.42 (sext, 4H, –SC_2H_4–C**H**$_2$–CH_3), 0.93 (t, 6H, SC_3H_6–C**H**$_3$). 0.92 (s, 3H, C**H**$_3$–(CH_2–ester–)$_3$).

^{13}C NMR (400 MHz, $CDCl_3$) δ in ppm: 222.0 (C=S), 171.5 (C=O), 67.5 (C–O–C=O), 64.8 (HO–C–), 47.7 (ester–(CH_3)CH–S), 40.1 ((CH_3)C–(ester–)$_3$), 37.1 (–S–**C**–C_3H_7), 30.0 (–SC–**C**–C_2H_5), 22.2 (–SC_2–**C**–CH_3), 16.8 ((CH_3)CH–(ester–)$_3$), 16.6 (ester–(CH_3)CH–S), 13.7 (SC_3–**C**H_3).

Synthesis of DMA polymers by RAFT polymerization. DMA, RAFT agents, and AIPD were dissolved in the solvent (DMF: water = 90: 10). The monomer concentration and the ratio of reactants are shown in Table S1 (The ratio of [Trithiocarbonate]: [Initiator] = 1: 0.02). The solution was prepared in a glass tube and degassed by freeze-thaw cycles (three times). The glass

tube was sealed and put in an oil bath. The reaction proceeded at 70 °C for 3 h. The reaction was stopped by exposing the solution to air. The monomer conversion was determined using ^{1}H NMR measurement. The polymer solutions were diluted with MeOH (1 mL) and precipitated in Et_2O (twice). The polymers were dried *in vacuo* and obtained as yellow solids.

Trivalent star polymer (SD_n): ^{1}H NMR (400 MHz, D_2O) δ in ppm: 3.95 (brs, CH_3–(C**H**$_2$–ester–)$_3$), 3.34 (brs, –S–CH_2–C_3H_7), 3.10-2.70 ($CON(CH_3)_2$), 2.70–2.30 (brs, –CH– main chain), 1.90–1.20 (brd, –CH_2– main chain and –SCH_2–C_2**H**$_4$–CH_3), 1.03–0.90 (brd, ester–CH(C**H**$_3$)–S and C**H**$_3$–C–(CH_2–ester–)$_3$), 0.80 (SC_3H_6–C**H**$_3$).

Bivalent linear polymer (B-LD_n): ^{1}H NMR (400 MHz, D_2O) δ in ppm: 3.95 (brs, HO–CH_2–CCH_3–(C**H**$_2$–ester–)$_2$), 3.50–3.30 (brd, HO–C**H**$_2$–CCH_3–(CH_2–ester–)$_2$ and –S–C**H**$_2$–C_3H_7), 3.10-2.70 ($CON(CH_3)_2$), 2.70–2.30 (brs, –CH– main chain), 1.90–1.20 (brd, –CH_2– main chain and –SCH_2–C_2**H**$_4$–CH_3), 1.05 (brs, ester–CH(C**H**$_3$)–S), 0.95–0.80 (brd, HO–CH_2–CC**H**$_3$–(CH_2–ester–)$_2$ and SC_3H_6–C**H**$_3$).

Monovalent linear polymer (M-LD_{52}): ^{1}H NMR (400 MHz, D_2O) δ in ppm: 3.60 (brs, C**H**$_3$–ester–), 3.34 (brs –S–C**H**$_2$–C_3H_7), 3.10-2.70 (brd, $CON(CH_3)_2$), 2.70-2.30 (brs, –CH– main chain), 1.75-1.20 (brd, –CH_2– main chain and –SCH_2–C_2**H**$_4$–CH_3), 1.03 (brs, ester–CH(C**H**$_3$)–S), 0.81 (brs, SC_3H_6–C**H**$_3$).

End-modification of alkyne groups on trithiocarbonate groups of polymers. The DMA polymers (50 mg) were dissolved in dry THF (2 mL), and the polymer solution was bubbled with nitrogen for 10 min. Propargyl acrylate (30 mg, 274 μmol) and *n*-butylamine (20 mg, 274 μmol) were added, and the mixture was stirred for 6 h at room temperature under nitrogen atmosphere.

The polymer solutions were precipitated in Et_2O (twice). The polymers were dried *in vacuo* and obtained as white solids.

Trivalent star polymer (SD_nA): ^1H NMR (400 MHz, D_2O) δ in ppm: 3.95 (brs, CH_3–(C**H**$_2$–ester–)$_3$), 3.60 (brs, –C≡C**H**), 3.10-2.70 ($CON(CH_3)_2$ and –S–C**H**$_2$–C**H**$_2$–ester), 2.70–2.30 (brs, –CH– main chain), 1.90–1.20 (brd, –CH_2– main chain), 1.03–0.96 (brd, ester–CH(C**H**$_3$)–S and C**H**$_3$–C–(C**H**$_2$–ester–)$_3$).

Bivalent linear polymer (B-LD_nA): ^1H NMR (400 MHz, D_2O) δ in ppm: 4.00 (brs, HO–CH_2–CCH_3–(C**H**$_2$–ester–)$_2$), 3.65 (brd, –C≡C**H**), 3.45 (brs, HO–C**H**$_2$–CCH_3–(CH_2–ester–)$_2$), 3.10-2.70 ($CON(CH_3)_2$ and –S–C**H**$_2$–C**H**$_2$–ester), 2.70–2.30 (brs, –CH– main chain), 1.90–1.20 (brd, –CH_2– main chain and –SCH_2–C_2**H**$_4$–CH_3), 1.05 (brs, ester–CH(C**H**$_3$)–), 0.95 (brs, HO–CH_2–CC**H**$_3$–(CH_2–ester–)$_2$).

Monovalent linear polymer (M-$LD_{52}A$): ^1H NMR (400 MHz, D_2O) δ in ppm: 3.58 (brs, C**H**$_3$–ester– and –C≡C**H**), 3.10-2.70 (brd, $CON(CH_3)_2$ and –S–C**H**$_2$–C**H**$_2$–ester), 2.70-2.30 (brs, –CH– main chain), 1.75-1.20 (brd, –CH_2– main chain), 1.03 (brs, ester–CH(C**H**$_3$)–).

Glycomodification on polymer terminals by copper-catalyzed azide-alkyne cycloaddition. The DMA polymers with alkyne terminals (20 mg), 6'-SALac azide (10 mg, 15 μmol), $CuSO_4$ (0.8 mg, 5 μmol) were dissolved in the mixture of H_2O (800 μL) and MeCN (750 μL). Sodium L-ascorbate (2 mg, 10 μmol) in H_2O (200 μL) was added, and the mixture was bubbled with nitrogen for 15 min. The tip of needle was pulled above the liquid level, and the mixture was stirred for 24 h at room temperature under nitrogen atmosphere. The objective was purified by dialysis (MWCO = 3,500) against water, and was obtained after freeze-drying.

Trivalent star glycoligand (SD_nG): ^1H NMR (400 MHz, D_2O) δ in ppm: 8.22 (s, triazole), 5.70 (d, H-1), 5.21 (s, O–C**H**$_2$–triazole), 4.38 (d, H-1'), 4.05-3.42 (m, sugar-H and CH_3–(C**H**$_2$–ester–)$_3$), 3.10-2.70 ($CON(CH_3)_2$, –S–C**H**$_2$–C**H**$_2$–ester and H-3"$_{eq}$), 2.70–2.30 (brs, –CH– main chain), 1.92 (s, NHCO–C**H**$_3$), 1.72–1.16 (brd, H-3"$_{ax}$ and –CH_2– main chain), 1.08–0.93 (brd, ester–CH(C**H**$_3$)– and C**H**$_3$–C–(CH_2–ester–)$_3$).

Bivalent linear glycoligand (B-LD_nG): ^1H NMR (400 MHz, D_2O) δ in ppm: 8.22 (s, triazole), 5.70 (d, H-1), 5.21 (s, O–C**H**$_2$–triazole), 4.38 (d, H-1'), 4.05-3.42 (m, sugar-H and HO–C**H**$_2$–CCH_3–(C**H**$_2$–ester–)$_2$), 3.10-2.70 ($CON(CH_3)_2$, –S–C**H**$_2$–C**H**$_2$–ester and H-3"$_{eq}$), 2.70–2.30 (brs, –CH– main chain), 1.92 (s, NHCO–C**H**$_3$), 1.72–1.16 (brd, H-3"$_{ax}$ and –CH_2– main chain), 1.08–0.93 (brd, ester–CH(C**H**$_3$)– and HO–CH_2–CC**H**$_3$–(CH_2–ester–)$_2$).

Monovalent linear glycoligand (M-$LD_{52}G$): ^1H NMR (400 MHz, D_2O) δ in ppm: 8.22 (s, triazole), 5.70 (d, H-1), 5.21 (s, O–C**H**$_2$–triazole), 4.38 (d, H-1'), 4.05-3.42 (m, sugar-H and C**H**$_3$–ester–), 3.10-2.70 ($CON(CH_3)_2$, –S–C**H**$_2$–C**H**$_2$–ester and H-3"$_{eq}$), 2.70–2.30 (brs, –CH– main chain), 1.92 (s, NHCO–C**H**$_3$), 1.72–1.16 (brd, H-3"$_{ax}$ and –CH_2– main chain), 1.02 (brs, ester–CH(C**H**$_3$)–).

Cleavage of polymer arms of glycoligands. $SD_{41}G$ and **$LD_{39}G$** (2 mg) were dissolved in NaOH aq (0.2 M, 1 mL), respectively. The solutions were incubated at 70 °C for 1 h, and then, HCl aq (0.2 M, 1 mL) was added to neutralize the solutions. The samples were analysed by SEC system without purification.

Hemagglutination inhibition (HI) assay. Phosphate-buffered saline (PBS) was added into a 96-well plate (25 μL/well) except the first lane. Glycoligand solution (4 mg/mL, 50 μL) was injected in the first lane. The solution in the first lane were twofold serially diluted (25 μL/well).

Influenza virus solution [A/Panama/2007/99 (H3N2) or A/Puerto Rico/8/34 (H1N1), 4 HAU] was injected in each well (25 μL/well). The 96-well plate was incubated for 1 h at 4 °C. Red blood cells in the purchased blood cell suspension were washed by centrifugation with PBS three times. The concentrated red blood cells were resuspended in PBS (0.5 v/v%) and was injected in each well (50 μL). The 96-well plate was incubated for 1 h at 4 °C (n = 3). Precipitation of red blood cells was determined by visual inspection.

Results and Discussion

Prediction of Polymer Length using Theoretical Models. To predict the appropriate polymer structure to enable the multivalent binding to the three CRDs of HA, the polymer length of the star polymer arms (distance from the cross-linked point to the polymer terminals) was calculated based on the Gaussian model. The theoretical models of synthetic polymers are based on their ideal states, and conformation of the synthetic polymers in a solution does not correspond to the theoretical conformation unless in the theta states. This indicates that the conformation of the objective star polymers in an aqueous solution would not match that of the theoretical models; however, the theoretical prediction based on the classical model is still useful as a guideline for designing the polymer ligand. A linear polymer based on the Gaussian model was initially considered.[38] The distance between the polymer terminals in one polymer molecule ‹*R*› was estimated using the following equation:

$$\langle R^2 \rangle = CNb^2 \text{——} (1)$$

where *C* is the characteristic ratio of monomer (*N*,*N*-dimethylacrylamide model (DMA)： 9.2),[39] *N* is the C−C bond number of the polymer backbone, and b is the C−C bond length (0.154 nm). The gyroid radius of a linear polymer (‹*S*›$_{lin}$) is calculated using the equation:

$$\langle S^2 \rangle_{lin} = \langle R \rangle^2/6 \text{——} (2)$$

and that of a star polymer (‹*S*›$_{star}$) is obtained by multiplying the shrinking ratio (g_s):

$$g_s = (3f-2)/f^2 \text{——} (3)$$

$$\langle S^2 \rangle_{star} = g_s \langle S^2 \rangle_{lin} \text{——} (4)$$

where f is number of polymer arms (for triarm star polymers, $f = 3$). The relationship between the number of monomer units of the polymer arm and the gyroid radius is shown in Figure 1a. The CRDs of HA are located at the vertices of a triangle, and the distance between two CRDs of HA is 4.5 nm.[25] The distance from the center of the triangle to the CRD (d_r) is 2.6 nm (Figure 1b, c). Thus, the theoretical prediction suggested that a star polymer with a degree of polymerization (DP) of 40 would have a comparable gyroid radius to the arrangement of CRDs on the HA surface. The designed star polymer was expected to display the glycoepitopes near the three CRDs, resulting in effective multivalent binding.

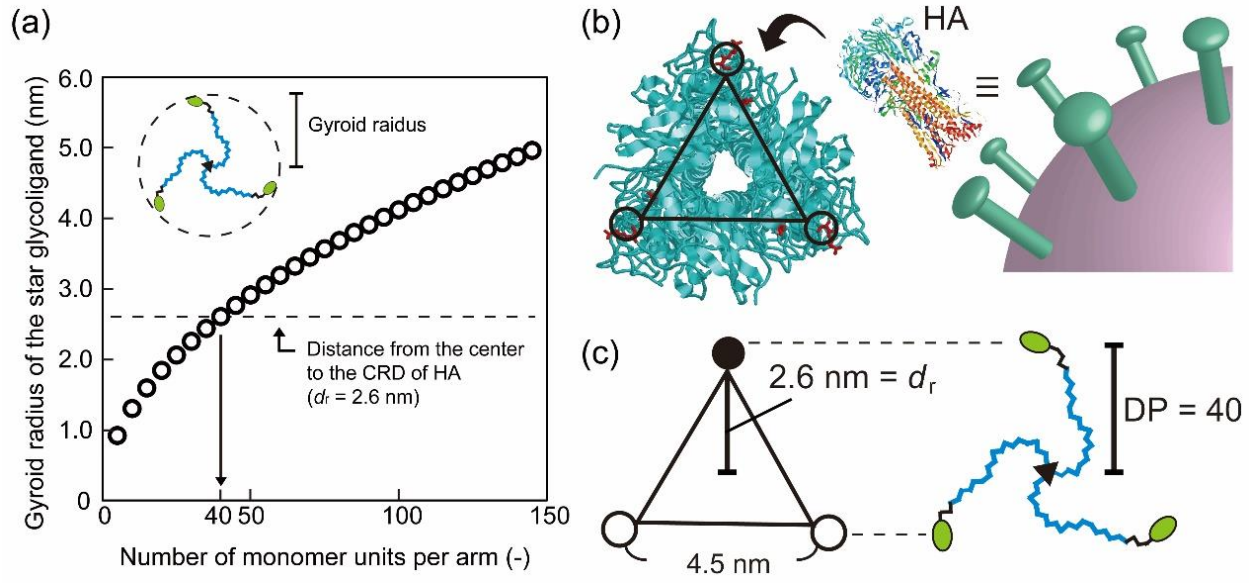

Figure 1. (a) Estimated gyroid radius of star glycoligands with different numbers of monomer units per arm. (b) The structures of hemagglutinin (PDB: 5HMG) and a surface illustration of the influenza virus. The amino acids involved in the interaction with sialic acids are shown in red. (c) Arrangement of the CRDs of HA as a triangle (left) and the star glycoligand with the appropriate DP (right). The circles indicate the CRDs on HA. The distance between two pockets is 4.5 nm. The distance from the center to the CRD is 2.6 nm, and is defined as d_r.

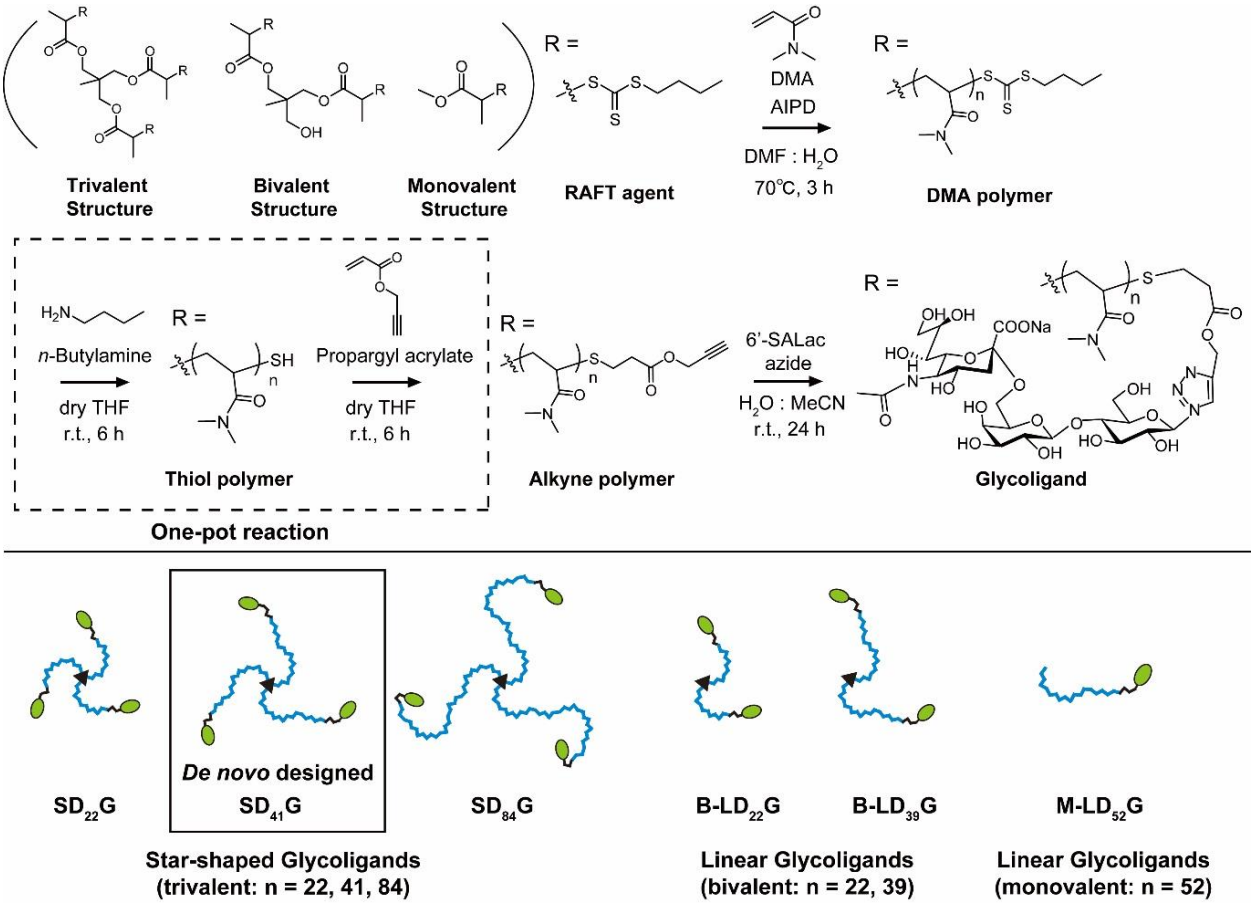

Figure 2. (Top) Schematic illustration of the synthesis of glycoligands by RAFT polymerization and functional modification onto the polymer terminals. (Bottom) Illustrations of the synthesized glycoligands with different DP and topologies.

Synthesis of Well-Defined Glycoligands with the Predicted Structure. A schematic illustration of the synthesis of the glycoligands is shown in Figure 2. The hydrophilic star polymer with trivalent arms was synthesized by RAFT polymerization of DMA with a trifunctional RAFT agent (the polymer is abbreviated to SD below). DMA was chosen as the

monomer owing to its inertness to biomolecular recognition.[34] To obtain star polymers with a DP of 40, the target DP was set at 50 based on the limited conversion rate of star polymers in RAFT polymerization (conversion rate = 80% in a previous study).[35] The ratio of [RAFT agent]: [initiator (AIPD)] was fixed at 20: 1 to avoid the undesired termination reaction.[9,40] The polymerization proceeded at 70 °C for 3 h in a mixture of DMF and water (the detailed conditions are shown in Table S1). The conversion rate of SD polymer was 82% from the proton nuclear magnetic resonance (^{1}H NMR) spectrum (Table 1). After purification, methyl protons both at butyl groups of the RAFT terminals and at the cross-linked point of the star polymer structure were observed at 0.81 and 0.96 ppm in the ^{1}H NMR spectrum, respectively (Figure S1-6). This indicates that the RAFT terminals and the cross-linked structure in the SD polymer were maintained. The DP of the SD polymer was calculated to be 41 from the integral values of the main chain peaks in the ^{1}H NMR spectrum. This value corresponds with the theoretical DP (the target DP × conversion rate: 50 × 0.82 = 41). Size exclusion chromatographs of the SD polymer showed a narrow unimodal peak (Figure 3a, M_w/M_n = 1.14). These results indicate that a well-defined star DMA polymer with a DP of 41 was obtained (abbreviated to **SD_{41}**). As control samples, trivalent star DMA polymers with different DP (**SD_{22}** and **SD_{84}**), bivalent linear DMA polymers (**B-LD_{22}** and **B-LD_{39}**), and monovalent linear DMA polymer (**M-LD_{52}**) were prepared in the same procedure (Table 1, Figure 3a, S1 and S2a).

Table 1. Properties of RAFT polymerization of DMA.

Polymer[a]	[M]:[Trithio]:[Ini]	Conv.[b]	DP[c]	Alkyne modification[c]	$M_{n,NMR}$[d]	$M_{n,SEC}$[e]	$M_{w,SEC}$[e]	M_w/M_n[e]
		(%)	(mer)	(%)	(g/mol)	(g/mol)	(g/mol)	
SD_{22}	30: 1: 0.02	71	22	–	7,300	4,500	5,000	1.12
$SD_{22}A$		–	–	84	–	3,700	5,400	1.45
SD_{41}	50: 1: 0.02	82	41	–	13,000	9,200	10,500	1.14
$SD_{41}A$		–	–	93	–	7,700	10,600	1.37
SD_{84}	100: 1: 0.02	85	84	–	25,800	21,100	23,400	1.11
$SD_{84}A$		–	–	88	–	18,100	22,900	1.26
B-LD_{22}	25: 1: 0.02	86	35	–	4,900	3,300	3,700	1.11
B-$LD_{22}A$		–	–	94	–	3,600	4,000	1.11
B-LD_{39}	50: 1: 0.02	80	56	–	8,300	5,900	6,700	1.14
B-$LD_{39}A$		–	–	88	–	5,700	7,100	1.24
M-LD_{52}	50: 1: 0.02	>99	52	–	5,200	3,600	4,900	1.14
M-$LD_{52}A$		–	–	89	–	4,100	4,700	1.14

(a) The star DMA polymer with DP of 22 is abbreviated to SD_{22}. The bivalent linear DMA polymer with DP of 22 is abbreviated to B-LD_{22}. The monovalent linear DMA polymer with DP of 52 is abbreviated to M-LD_{52}. (b) The conversion rate was determined from ^{1}H NMR. (c) The DP of each polymer arm and the percentage of alkyne group on the polymer terminals were determined from ^{1}H NMR spectra. (d) The molecular weight was calculated using the equation: $M_{n,NMR} = f \times (MW_{DMA} \times DP_{DMA}) + MW_{RAFT}$. f = 3, 2, and 1 for SD, B-LD, and M-LD, respectively. (e) The molecular weights were determined by size exclusion chromatography (SEC) analysis. The eluent was DMF with 10 mM LiBr. The calibration was performed with polystyrene standards. M_w/M_n was calculated using the values from SEC analysis.

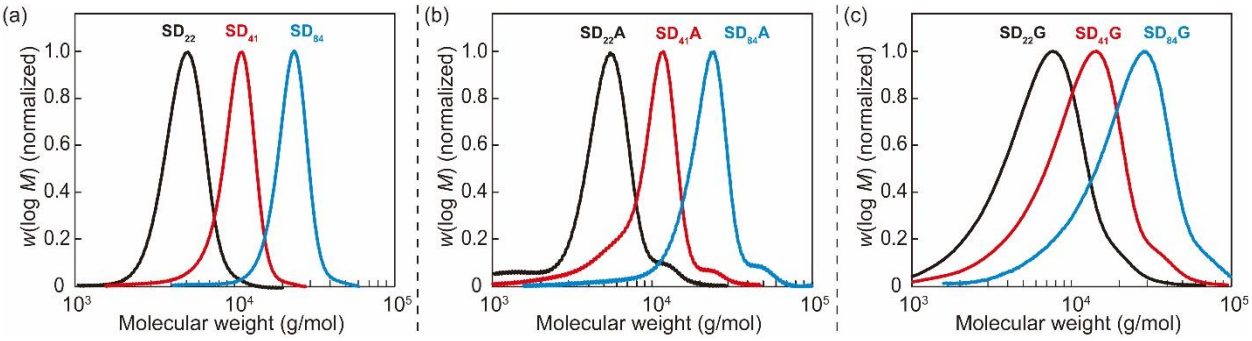

Figure 3. Size exclusion chromatographs of (a) star DMA polymers (SD_{22}, SD_{41}, and SD_{84}), (b) star DMA polymers with alkyne terminal ($SD_{22}A$, $SD_{41}A$, and $SD_{84}A$), and (c) star glycoligands ($SD_{22}G$, $SD_{41}G$, and $SD_{84}G$). The eluents were DMF with 10 mM LiBr for (a) and (b), and water with 100 mM $NaNO_3$ for (c). The analyses were calibrated by polystyrene standards for (a) and (b), and by pullulan standards for (c).

The terminal trithiocarbonate groups of the synthesized polymers were converted to alkyne groups in a one-pot procedure.[41] The polymers were dissolved in dry THF with an excess of *n*-butylamine and propargyl acrylate, and were stirred for 6 h under an atmosphere of nitrogen. The trithiocarbonate groups were decomposed to thiol groups, and then the thiol–ene reaction with propargyl acrylate proceeded (Figure 2). The removal of trithiocarbonate was confirmed by the disappearance of its absorbance peak (λ = 310 nm) in the UV spectra (Figure S3). The addition of alkyne groups at the polymer terminals was supported by ^{1}H NMR. The peak of methylene protons adjacent to the alkyne group was identified using $CDCl_3$ as the solvent (Figure S1). The calculated yields of alkyne modification using the integral values for the proton peaks were around 90% for all polymers (Table 1). The yield was slightly lower than 100% owing to the formation of disulfide linkages between the polymer arms during the one-pot reaction. The

intermolecular formation of disulfide linkage was suggested by the shoulder peaks of higher molecular weight in the SEC curves (Figure 3b).[41] These results indicate that DMA polymers with alkyne terminals (**$SD_{22}A$**, **$SD_{41}A$**, **$SD_{84}A$**, **B-$LD_{22}A$**, **B-$LD_{39}A$**, and **M-$LD_{52}A$**) were obtained.

The 6'-SALac epitope for influenza hemagglutinin was used in this study. 6'-SALac is a trisaccharide with the Neu5Ac-α(2,6)-Gal structure that is recognized by influenza hemagglutinins of human-types.[42] The anomeric hydroxyl group of 6'-SALac was converted to an azide group using a method described in a previous report,[43] and 6'-SALac azide was conjugated to the alkyne terminals of the polymer arms using the copper-catalyzed azide-alkyne cycloaddition (Figure 2). The appearance of the peak of the triazole ring in the ^{1}H NMR spectra of the obtained glycoligands indicated the successful introduction of 6'-SALac (Figure S1 and

Table 2. Properties of synthesized glycoligands.

Ligand[a]	DP[b]	Glycoepitope modification[b]	$M_{n,SEC}$[c]	$M_{w,SEC}$[c]	M_w/M_n[c]	R_h[d]	PDI[e]
	(mer)	(%)	(g/mol)	(g/mol)		(nm)	(-)
$SD_{22}G$	22	90	5,600	7,500	1.35	2.0 ± 0.02	0.31
$SD_{41}G$	41	90	9,800	12,900	1.32	2.8 ± 0.09	0.41
$SD_{84}G$	84	88	21,000	26,800	1.28	3.9 ± 0.07	0.39
B-$LD_{22}G$	35	93	3,600	4,800	1.34	1.9 ± 0.05	0.45
B-$LD_{39}G$	56	92	5,900	7,900	1.35	2.4 ± 0.13	0.41
M-$LD_{52}G$	52	83	3,600	4,900	1.36	2.0 ± 0.09	0.44

(a) The star glycoligand with DP of 22 is abbreviated to $SD_{22}G$. The bivalent linear glycoligand with DP of 22 is abbreviated to B-$LD_{22}G$. The monovalent linear glycoligand with DP of 52 is abbreviated to M-$LD_{52}G$. (b) The DP of each polymer arm and the percentage of 6'-SALac on the polymer terminals were determined by ^{1}H NMR. (c) The molecular weights were determined by size exclusion chromatography (SEC) analysis. The eluent was water with 100 mM $NaNO_3$. The calibration was performed with pullulan standards. M_w/M_n was calculated using the values from SEC analysis. (d) The hydrodynamic radius (R_h) was estimated by dynamic light scattering (DLS) measurement in PBS (-) buffer (3 g/L). The temperature was 25 °C. (e) Polydispersity index of DLS measurement.

Table 2). Although the yields of the glycoepitope modification are summarized in Table 2, it should be noted that NMR integration of the proton peaks involves an error in quantification due to their low content in the polymers. SEC analysis showed the unimodal peaks for all the glycoligands with relatively narrow dispersity (Table 2, Figure 3c and S2). These results demonstrate that glycoligands with one glycoepitope on each polymer arm were obtained (**$SD_{22}G$**, **$SD_{41}G$**, **$SD_{84}G$**, **B-$LD_{22}G$**, **B-$LD_{39}G$**, and **M-$LD_{52}G$**).

Confirmation of the Cross-linked Structures of the Glycopolymers. To confirm the presence of cross-linked points in the synthesized glycoligands, the ester bonds adjacent to the center of the glycoligand structures were hydrolyzed in basic conditions. **$SD_{41}G$** and **B-$LD_{39}G$** were dissolved in 0.2 M NaOH(aq) at 2.0 g/L and were incubated at 70 °C for 2 h. After the treatment, the hydrolyzed glycoligands were analyzed by SEC (Figure 4). The hydrolyzed samples showed narrow unimodal peaks with smaller molecular weight than before hydrolysis, indicating that **$SD_{41}G$** and **B-$LD_{39}G$** originally had cross-linked structures. Furthermore, both hydrolyzed samples showed the same molecular weights (M_n = 3,200 g/mol), which corresponds with the finding that the DP of the polymer arms of **$SD_{41}G$** and **B-$LD_{39}G$** was almost the same (DP = 41 and 39, respectively). These results indicate that the synthesized glycoligands had the cross-linked structures anticipated for the chosen multivalent RAFT agents.

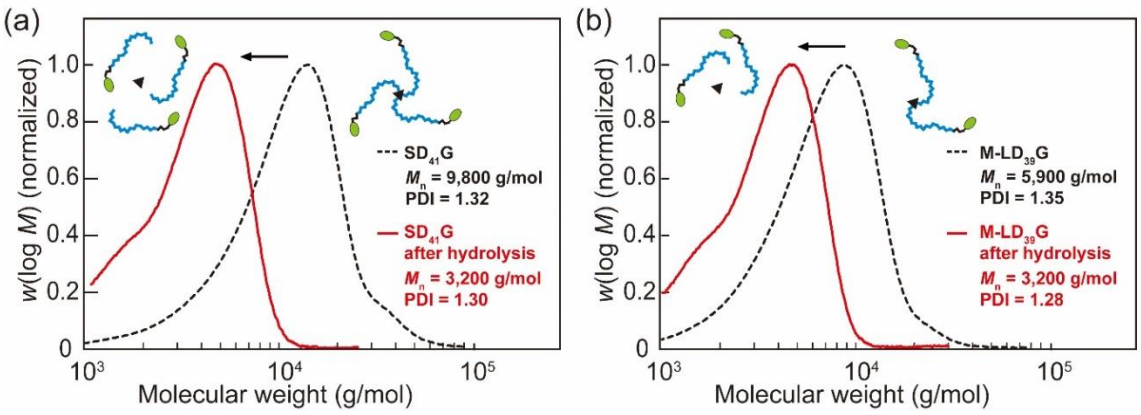

Figure 4. Size exclusion chromatographs of (a) **SD$_{41}$G** and (b) **B-LD$_{39}$G** glycoligands before (black dashed lines) and after (red lines) hydrolysis. The eluent was water with 100 mM $NaNO_3$, and the system was calibrated by pullulan standards.

Characterization of the Glycoligands by Dynamic Light Scattering. To evaluate the precision of the molecular design of the synthesized glycoligands, their hydrodynamic radii (R_h) in phosphate buffer saline (PBS) solution were measured using dynamic light scattering (DLS). The R_h of the star glycoligands were 2.0, 2.8, and 3.9 nm for **SD$_{22}$G**, **SD$_{41}$G**, and **SD$_{84}$G**, respectively (Table 2 and Figure S4-1). The R_h of the linear glycoligands were 1.9, 2.4, and 2.0 nm for **B-LD$_{22}$G**, **B-LD$_{39}$G**, and **M-LD$_{52}$G**, respectively (Table 2 and Figure S4-2). These results indicate that the R_h of the synthesized glycoligands increased with the DP of the polymer arms, and that the R_h of **SD$_{41}$G** and **B-LD$_{39}$G** were close to the distance from the center of the triangle to the CRD of HA (d_r = 2.6 nm) as expected in the Gaussian model calculated before the synthesis (Figure 5). This demonstrated that the structures of the glycoligands were well-controlled on the nano-meter scale by living radical polymerization.

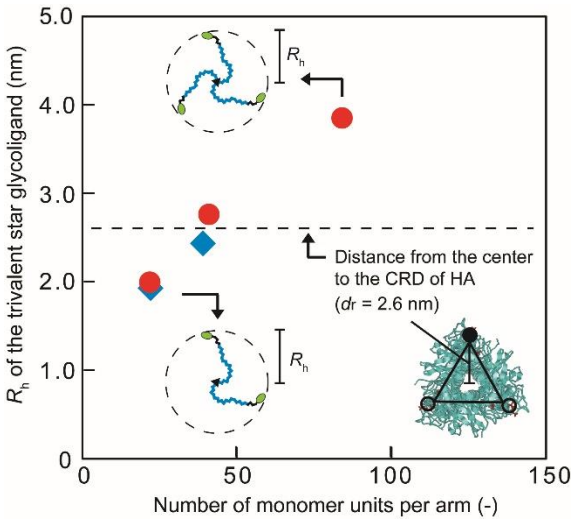

Figure 5. The hydrodynamic radius (R_h) of star (red circles) and linear (blue rhombus) glycoligands with different number of monomer units per polymer arm with illustrations of the glycoligands and HA.

Evaluation of the Interaction with the Influenza Virus by hemagglutination Inhibition Assay. The interactions of the synthesized glycoligands with the influenza virus were evaluated using a hemagglutination inhibition (HI) assay. Fetuin, a natural glycoprotein, and **SD$_{41}$**, which has no glycoepitopes, were used as the positive and negative controls, respectively. **SD$_{22}$G**, **SD$_{41}$G**, **SD$_{84}$G**, **B-LD$_{22}$G**, and fetuin inhibited the aggregation of red blood cells (RBCs) caused by the virus (A/Panama/2007/99, H3N2), demonstrating their interactions with HA on the virus (Figure S5A). **B-LD$_{39}$G** and **M-LD$_{52}$G** did not show HI in the concentration range of this work. **SD$_{41}$** did not inhibit the RBC aggregation, indicating the absence of non-specific interaction between the DMA segment and HA. The selectivity of the glycoligands for the virus type based on the glycoepitopes was confirmed by an HI assay using the other influenza virus strain (A/Puerto Rico/8/34, H1N1). A/Puerto Rico/8/34, H1N1 has selectivity for the Neu5Ac-α-(2,3)-

Gal structure, not the Neu5Ac-α-(2,6)-Gal structure.[44] Thus, the glycoligands displaying 6'-SALac (Neu5Ac-α-(2,6)-Gal structure) were not expected to interact with this different virus strain. As anticipated, the glycoligands did not inhibit the aggregation of RBCs, while fetuin did because both types of carbohydrate structure are displayed on fetuin. These results demonstrate that the selectivity of the glycoepitopes in the glycoligands was maintained, and that the glycoligands would act as inhibitors against the influenza virus.

The minimum ligand concentration for HI with the virus strain (A/Panama/2007/99, H3N2) was defined as the inhibition constant (K_i), and the K_i was calculated in terms of glycoepitope concentration (Figure 6a). The average values of K_i for **SD$_{22}$G**, **SD$_{41}$G**, **SD$_{84}$G**, **B-LD$_{22}$G** and fetuin were 112, 35, 163, 91 and 19 μM, respectively (Table 3). The interaction of the monovalent glycoepitopes with HA was evaluated using 6'-SALac (K_i = 20 mM, Figure S5). The lower K_i values of the glycoligands indicate that their interactions with HA were stronger than that of 6'-SALac. The order of the strength of the interaction was **SD$_{41}$G** > **B-LD$_{22}$G** = **SD$_{22}$G** > **SD$_{84}$G**. The interaction of the glycoligands with HA was enhanced by the cluster glycoside effect. The strongest interaction with HA, which was observed for **SD$_{41}$G**, is attributed to the multivalent binding to more CRDs of HA than the other glycoligands owing to the polymer length of **SD$_{41}$G** being designed for the d_r on HA (= 2.6 nm, Figure 1c and 6b). The smaller-than-2,6 nm R_h of **SD$_{22}$G** led to insufficient valency in binding to the three CRDs of HA, resulting in bivalent binding. Conversely, **SD$_{84}$G** had a larger R_h than 2.6 nm and the arrangement of the glycoepitopes did not correspond to that of the CRDs. Since the DMA polymer arms were flexible and the polymer length was longer than 2.6 nm, **SD$_{84}$G** was expected to be able to achieve trivalent binding. However, trivalent binding of **SD$_{84}$G** was unfavorable in terms of entropic loss and was rarely achieved, resulting in a weaker interaction. **B-LD$_{22}$G** had

the same R_h as **SD$_{22}$G**, and the interaction with HA was to the same extent as for **SD$_{22}$G** suggesting bivalent binding. The R_h of **B-LD$_{39}$G** was close to 2.6 nm as well as to the R_h of **SD$_{41}$G**; however, the interaction of **B-LD$_{39}$G** was weaker than that of **B-LD$_{22}$G** (K_i of **B-LD$_{39}$G** was not determined in this work). This is attributed to the difference in molecular mobility of the polymer arms between the star structure (**SD$_{41}$G**) and the linear structure (**B-LD$_{39}$G**). Furthermore, **B-LD$_{22}$G** exhibited a stronger interaction than **SD$_{84}$G** even though the glycoepitope valency of **B-LD$_{22}$G** (= 2) was lower than that of the star glycoligands (= 3), indicating that the glycoepitope valency was not only factor in determining the interactions with HA, and that both of the glycoepitope arrangement and the molecular mobility are important. **M-LD$_{52}$G**, with the monovalent glycoepitope, did not enable multivalent interaction and the K_i value was not sufficient to be determined. These results indicate that the designed star glycoligand **SD$_{41}$G**, which had a comparable hydrodynamic radius to d_r, showed the strongest interaction with HA. This demonstrated that the *de novo* design of the synthetic polymer structures enabled control of the biomolecular functions of the glycoligand, and that the precision level of synthetic polymer structures as nanomaterials can be comparable to those of DNA and peptides.

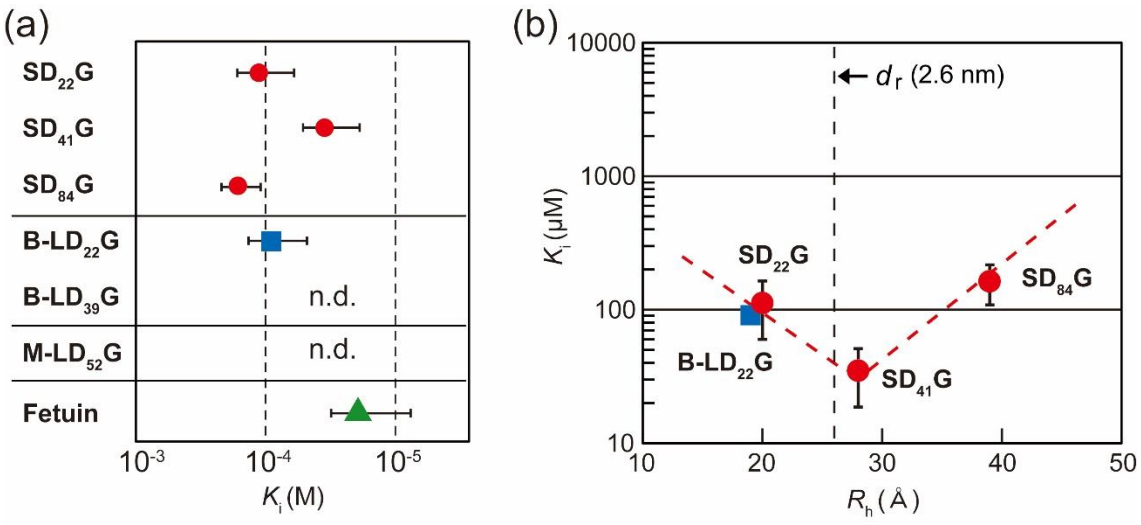

Figure 6. (a) K_i of the glycoligands and fetuin against influenza viruses [A/Panama/2007/99 (H3N2)] from the HI assay (n = 3). The values were calculated in the glycoepitope concentration. (b) K_i against hydrodynamic radius (R_h). For (b), the red circles and blue square represent the star and linear glycoligands, respectively.

The binding modes between the glycoligands and HA were estimated using the following formula suggested by Whitesides and co-workers.[45]

$$K_N{}^{poly} = (K^{mono})^{\alpha N} \quad \text{—— (5)}$$

Where $K_N{}^{poly}$ and K^{mono} indicate the association constants of polyvalent interaction and monovalent interaction, respectively. N is the number of binding sites in the interaction between a polyvalent ligand and a receptor, and α is the degree of cooperativity. Although the K_i from the HI assay is not the association constant (K_a), correlation between K_a and K_i in the interaction of glycoligands with lectins has previously been suggested.[46] Thus, assuming that the K_i reflects K_a between the glycoligands and HA, the number of binding sites was estimated. The constants of

the star glycoligands and 6'-SALac in the interactions with HA (K_N^{poly} and K^{mono}) were calculated as the inverse of the K_i. For example, K_i of 6'-SALac was 20 mM, and K^{mono} was calculated as 50 M^{-1}. *N* for the glycoligands was calculated from formula (5) assuming α = 1 (Table 3). A rationale is provided in the Supporting Information. *N* for **SD$_{22}$G**, **SD$_{41}$G**, **SD$_{84}$G** and **B-LD$_{22}$G** was estimated to be 2.3, 2.6, 2.2, and 2.4, respectively. As one HA molecule has three CRDs, these values are reasonable. The suggested binding modes are summarized in Figure 7. Although the glycoepitope valency of **B-LD$_{22}$G** was two, *N* of **B-LD$_{22}$G** was 2.4. It is thought that the degree of cooperativity (α) would be different for the trivalent star and the bivalent linear structures owing to their molecular mobilities, and that *N* of **B-LD$_{22}$G** was therefore overestimated. This estimation of binding modes supported the interactions of the glycoligands being based on multivalent binding, and the binding modes being controlled by the molecular design of the synthetic polymers.

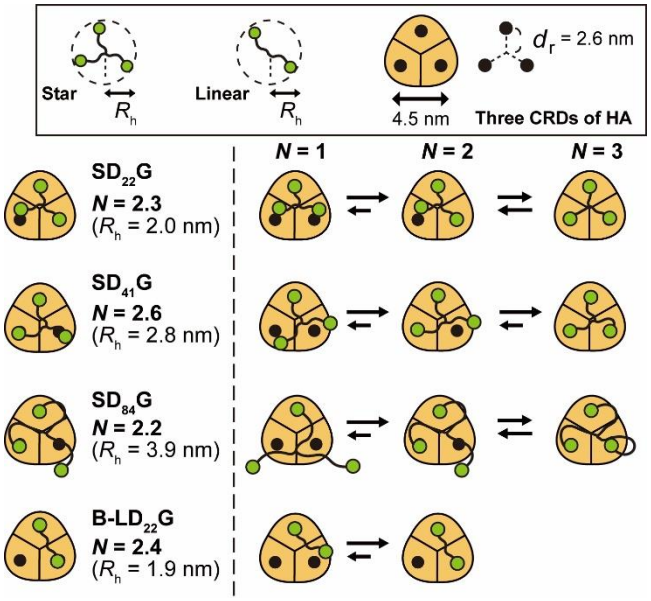

Figure 7. Illustration of the expected binding modes between the glycoligands and HA. R_h and *N* indicate the hydrodynamic radius and the number of binding sites for each ligand, respectively.

Table 3. Summary of the constants calculated with K_i for HA.

Ligand	K_i	K_N^{poly}	N^a
	(M)	(M^{-1})	(-)
$SD_{22}G$	1.12×10^{-4}	8930	2.3
$SD_{41}G$	3.49×10^{-5}	28680	2.6
$SD_{84}G$	1.63×10^{-4}	6150	2.2
B-$LD_{22}G$	9.11×10^{-5}	10980	2.4
B-$LD_{39}G$	n.d.	n.d.	n.d.
M-$LD_{52}G$	n.d.	n.d.	n.d.
Fetuin	1.93×10^{-5}	51870	2.8

The association constant was calculated using the formula: $K_N^{poly} = 1/K_i$. (a) N was determined using the formula $K_N^{poly} = (K^{mono})^{\alpha N}$, assuming $\alpha = 1$ and $K^{mono} = 50\ M^{-1}$ from K_i of 6'-SALac (20 mM).

Conclusions

We designed star-shaped glycoligands as effective inhibitors for hemagglutinin of the influenza virus. Prior to the synthesis, the Gaussian model of synthetic polymers provided a prediction of the appropriate polymer length, and a degree of polymerization of 40 was expected to achieve a polymer length that would match the arrangement of the carbohydrate recognition domains of hemagglutinin. Based on the prediction, a hydrophilic star polymer was synthesized by RAFT polymerization, and subsequent modification with 6'-sialyllactose at the polymer terminals provided the star-shaped glycoligands. The structures of the star-shaped glycoligands were well-controlled on the nano-meter scale, and the hydrodynamic radius of the star glycoligand with the predicted polymer length (**$SD_{41}G$**) was close to the distance from the center of the triangle to the CRD of HA. In the hemagglutination inhibition assay, the interaction of the glycoligand with the

predicted structure was the strongest among the synthesized glycoligands, suggesting effective multivalent binding to HA. The results in this work demonstrated that the structures of the synthetic polymers were well-controlled by living radical polymerization, and that their biological function (intermolecular recognition) was also controlled by the defined polymer structures. This work is expected to contribute to the development of novel nanomaterials using synthetic polymers that are comparable to or exceed the capabilities of natural biopolymers such as DNA and peptides. In particular, facile access to the preparation of synthetic polymers on a large scale would provide significant advantages in terms of pandemic threat, where immediate response is required. We hope that synthetic polymers will open up new opportunities in nano- and biotechnology.

ASSOCIATED CONTENT

The Supporting Information is available free of charge on the website at DOI: ---.

Additional details on the experimental methods; Spectra of ^{1}H NMR, ^{13}C NMR, and UV absorbance, results of the size exclusion chromatography, dynamic light scattering, HI assay (PDF).

AUTHOR INFORMATION

Corresponding Author

Yoshiko Miura – Department of Chemical Engineering, Kyushu University, 744 Motooka Nishi-ku, Fukuoka 819-0395, Japan.

E-mail: miuray@chem-eng.kyushu-u.ac.jp

Masanori Nagao – The same address above.

E-mail: nagaom@chem-eng.kyushu-u.ac.jp

Author Contributions

M.N. and Y.M. designed the project, and M.N. wrote the manuscript. M.N. carried out the polymer synthesis and characterization experiments. A.Y. carried out the influenza virus experiments. T.M., Y.H., and T.S. provided advice to improve the manuscript.

Notes

The authors declare no competing financial interest.

ACKNOWLEDGMENT

This work was supported by a Grant-in-Aid for Scientific Research (B) (JP19H02766) and a Grant-in-Aid for Scientific Research on Innovative Areas (JP20H05230 and JP20H04825).

REFERENCES

(1) Rogers, W. B.; Shih, W. M.; Manoharan, V. N. Using DNA to Program the Self-Assembly of Colloidal Nanoparticles and Microparticles. *Nat. Rev. Mater.* **2016**, *1*, 16008.

(2) Matsuurua, K. Rational Design of Self-Assembled Proteins and Peptides for Nano- and Micro-Sized Architectures. *RSC Adv.* **2014**, *4* (6), 2942–2953.

(3) Luo, Q.; Hou, C.; Bai, Y.; Wang, R.; Liu, J. Protein Assembly: Versatile Approaches to Construct Highly Ordered Nanostructures. *Chem. Rev.* **2016**, *116* (22), 13571–13632.

(4) Sinha, N. J.; Langenstein, M. G.; Pochan, D. J.; Kloxin, C. J.; Saven, J. G. Peptide Design and Self-Assembly into Targeted Nanostructure and Functional Materials. *Chem. Rev.* **2021**, DOI: org/10.1021/acs.chemrev.1c00712.

(5) Lutz, J. F.; Lehn, J. M.; Meijer, E. W.; Matyjaszewski, K. From Precision Polymers to Complex Materials and Systems. *Nat. Rev. Mater.* **2016**, *1*, 16024.

(6) Polymeropoulos, G.; Zapsas, G.; Ntetsikas, K.; Bilalis, P.; Gnanou, Y.; Hadjichristidis, N. 50th Anniversary Perspective: Polymers with Complex Architectures. *Macromolecules* **2017**, *50* (4), 1253–1290.

(7) Grubbs, R. B.; Grubbs, R. H. 50th Anniversary Perspective: Living Polymerization–Emphasizing the Molecule in Macromolecules. *Macromolecules* **2017**, *50* (18), 6979–6997.

(8) Ouchi, M.; Sawamoto, M. 50th Anniversary Perspective: Metal-Catalyzed Living Radical Polymerization: Discovery and Perspective. *Macromolecules 2017*, *50* (7), 2603–2614.

(9) Perrier, S. 50th Anniversary Perspective: RAFT Polymerization–A User Guide. *Macromolecules* **2017**, *50* (19), 7433–7447.

(10) Huang, Z.; Noble, B. B.; Corrigan, N.; Chu, Y.; Satoh, K.; Thomas, D. S.; Hawker, C. J.; Moad, G.; Kamigaito, M.; Coote, M. L.; Boyer, C.; Xu, J. Discrete and Stereospecific Oligomers

Prepared by Sequential and Alternating Single Unit Monomer Insertion. *J. Am. Chem. Soc.* **2018**, *140* (41), 13392–13406.

(11) Jiang, K.; Han, S.; Ma, M.; Zhang, L.; Zhao, Y.; Chen, M. Photoorganocatalyzed Reversible-Deactivation Alternating Copolymerization of Chlorotrifluoroethylene and Vinyl Ethers under Ambient Conditions: Facile Access to Main-Chain Fluorinated Copolymers. *J. Am. Chem. Soc.* **2020**, *142* (15), 7108–7115.

(12) Barnes, J. C.; Ehrlich, D. J. C.; Gao, A. X.; Leibfarth, F. A.; Jiang, Y.; Zhou, E.; Jamison, T. F.; Johnson, J. A. Iterative Exponential Growth of Stereo- and Sequence-Controlled Polymers. *Nat. Chem.* **2015**, *7* (10), 810–815.

(13) Li, Z.; Ren, X.; Sun, P.; Ding, H.; Li, S.; Zhao, Y.; Zhang, K. Protecting-Group-Free Iterative Exponential Growth Method for Synthesizing Sequence-Defined Polymers. ACS Macro Lett. 2021, 10 (2), 223–230.

(14) Martens, S.; Landuyt, A.; Espeel, P.; Devreese, B.; Dawyndt, P.; Du Prez, F. Multifunctional Sequence-Defined Macromolecules for Chemical Data Storage. *Nat. Commun.* **2018**, *9*, 4451.

(15) Lee, J. M.; Koo, M. B.; Lee, S. W.; Lee, H.; Kwon, J.; Shim, Y. H.; Kim, S. Y.; Kim, K. T. High-Density Information Storage in an Absolutely Defined Aperiodic Sequence of Monodisperse Copolyester. *Nat. Commun.* **2020**, *11*, 56.

(16) Hoshino, Y.; Taniguchi, S.; Takimoto, H.; Akashi, S.; Katakami, S.; Yonamine, Y.; Miura, Y. Homogeneous Oligomeric Ligands Prepared via Radical Polymerization That Recognize and Neutralize a Target Peptide. *Angew. Chem. Int. Ed.* **2020**, *59* (2), 679–683.

(17) Dwek, R. A. Glycobiology: Toward Understanding the Function of Sugars. *Chem. Rev.* **1996**, *96* (2), 683–720.

(18) Poole, J.; Day, C. J.; Von Itzstein, M.; Paton, J. C.; Jennings, M. P. Glycointeractions in Bacterial Pathogenesis. *Nat. Rev. Microbiol.* **2018**, *16* (7), 440–452.

(19) Ambrosi, M.; Cameron, N. R.; Davis, B. G. Lectins: Tools for the Molecular Understanding of the Glycocode. *Org. Biomol. Chem.* **2005**, *3* (9), 1593–1608.

(20) Lundquist, J. J.; Toone, E. J. The Cluster Glycoside Effect. *Chem. Rev.* **2002**, *102* (2), 555–578.

(21) Kiessling, L. L.; Grim, J. C. Glycopolymer Probes of Signal Transduction. *Chem. Soc. Rev.* **2013**, *42* (10), 4476–4491.

(22) Cecioni, S.; Imberty, A.; Vidal, S. Glycomimetics versus Multivalent Glycoconjugates for the Design of High Affinity Lectin Ligands. *Chem. Rev.* **2015**, *115* (1), 525–561.

(23) Yilmaz, G.; Becer, C. R. Glycopolymer Code: Programming Synthetic Macromolecules for Biological Targeting. *Macromol. Chem. Phys.* **2020**, *221* (7), 1–3.

(24) Song, Y.; Chen, Y.; Li, P; Dong, C. M. Photoresponsive Polypeptide-Glycosylated Dendron Amphiphiles: UV-Triggered Polymersomes, OVA Release, and In Vitro Enhanced Uptake and Immune Response. *Biomacromolecules* **2020**, *21*, 5345–5357.

(25) Kiran, P.; Bhatia, S.; Lauster, D.; Aleksić, S.; Fleck, C.; Peric, N.; Maison, W.; Liese, S.; Keller, B. G.; Herrmann, A.; Haag, R. Exploring Rigid and Flexible Core Trivalent Sialosides for Influenza Virus Inhibition. *Chem. Eur. J.* **2018**, *24* (72), 19373–19385.

(26) Liese, S.; Netz, R. R. Quantitative Prediction of Multivalent Ligand-Receptor Binding Affinities for Influenza, Cholera, and Anthrax Inhibition. *ACS Nano* **2018**, *12* (5), 4140–4147.

(27) Kim, Y.; Hyun, J. Y.; Shin, I. Multivalent Glycans for Biological and Biomedical Applications. *Chem. Soc. Rev.* **2021**, *50* (18), 10567–10593.

(28) Bianculli, R. H.; Mase, J. D.; Schulz, M. D. Antiviral Polymers: Past Approaches and Future Possibilities. *Macromolecules* **2020**, *53* (21), 9158–9186.

(29) Neumann, G.; Noda, T.; Kawaoka, Y. Emergence and Pandemic Potential of Swine-Origin H1N1 Influenza Virus. *Nature* **2009**, *459* (7249), 931–939.

(30) Weis, W.; Brown, J. H.; Cusack, S.; Paulson, J. C.; Skehel, J. J.; Wiley, D. C. Structure of the Influenza Virus Haemagglutinin Complexed with Its Receptor, Sialic Acid. *Nature* **1988**, *333*, 426–431.

(31) Yamabe, M.; Kaihatsu, K.; Ebara, Y. Sialyllactose-Modified Three-Way Junction DNA as Binding Inhibitor of Influenza Virus Hemagglutinin. *Bioconjug. Chem.* **2018**, *29* (5), 1490–1494.

(32) Waldmann, M.; Jirmann, R.; Hoelscher, K.; Wienke, M.; Niemeyer, F. C.; Rehders, D.; Meyer, B. A Nanomolar Multivalent Ligand as Entry Inhibitor of the Hemagglutinin of Avian Influenza. *J. Am. Chem. Soc.* **2014**, *136* (2), 783–788.

(33) Nagao, M.; Fujiwara, Y.; Matsubara, T.; Hoshino, Y.; Sato, T.; Miura, Y. Design of Glycopolymers Carrying Sialyl Oligosaccharides for Controlling the Interaction with the Influenza Virus. *Biomacromolecules* **2017**, *18* (12), 4385–4392.

(34) Nagao, M.; Matsubara, T.; Hoshino, Y.; Sato, T.; Miura, Y. Synthesis of Various Glycopolymers Bearing Sialyllactose and the Effect of Their Molecular Mobility on Interaction with the Influenza Virus. *Biomacromolecules* **2019**, *20* (7), 2763–2769.

(35) Nagao, M.; Matsubara, T.; Hoshino, Y.; Sato, T.; Miura, Y. Topological Design of Star Glycopolymers for Controlling the Interaction with the Influenza Virus. *Bioconjug. Chem.* **2019**, *30* (4), 1192–1198.

(36) Sprong, E.; Leswin, J. S. K.; Lamb, D. J.; Ferguson, C. J.; Hawkett, B. S.; Pham, B. T. T.; Nguyen, D.; Such, C. H.; Serelis, A. K.; Gilbert, R. G. Ab Initio Emulsion Polymerization by RAFT-Controlled Self-Assembly. *Macromol. Symp.* **2005**, *38*, 2191–2204.

(37) Nagao, M.; Kurebayashi, Y.; Seto, H.; Tanaka, T.; Takahashi, T.; Suzuki, T.; Hoshino, Y.; Miura, Y. Synthesis of Well-Controlled Glycopolymers Bearing Oligosaccharides and Their Interactions with Influenza Viruses. *Polym. J.* **2016**, *48* (6), 745–749.

(38) Guttman, C. M.; DiMarzio, E. A. Rotational Isomeric Modeling of a Polyethylene-like Polymer between Two Plates: Connection to "Gambler's Ruin" Problem. *Macromolecules* **1982**, *15* (2), 525–531.

(39) Chee, K. K. Dependence of Glass Transition Temperature on Chain Flexibility and Intermolecular Interactions in Polymers. *J. Appl. Polym. Sci.* **1991**, *43* (6), 1205–1208.

(40) Gody, G.; Maschmeyer, T.; Zetterlund, P. B.; Perrier, S. Rapid and Quantitative One-Pot Synthesis of Sequence-Controlled Polymers by Radical Polymerization. *Nat. Commun.* **2013**, *4*, 2505.

(41) Qiu, X. P.; Winnik, F. M. Facile and Efficient One-Pot Transformation of RAFT Polymer End Groups via a Mild Aminolysis/Michael Addition Sequence. *Macromol. Rapid Commun.* **2006**, *27* (19), 1648–1653.

(42) Sassaki, G. L.; Elli, S.; Rudd, T. R.; Macchi, E.; Yates, E. A.; Naggi, A.; Shriver, Z.; Raman, R.; Sasisekharan, R.; Torri, G.; Guerrini, M. Human (α2→6) and Avian (α2→3) Sialylated Receptors of Influenza A Virus Show Distinct Conformations and Dynamics in Solution. *Biochemistry* **2013**, *52* (41), 7217–7230.

(43) Tanaka, T.; Nagai, H.; Noguchi, M.; Kobayashi, A.; Shoda, S. I. One-Step Conversion of Unprotected Sugars to β-Glycosyl Azides Using 2-Chloroimidazolinium Salt in Aqueous Solution. *Chem. Commun.* **2009**, *23*, 3378–3379.

(44) Suzuki, T.; Horiike, G.; Yamazaki, Y.; Kawabe, K.; Masuda, H.; Miyamoto, D.; Matsuda, M.; Nishimura, S. I.; Yamagata, T.; Ito, T.; Kida, H.; Kawaoka, Y.; Suzuki, Y. Swine Influenza Virus Strains Recognize Sialylsugar Chains Containing the Molecular Species of Sialic Acid Predominantly Present in the Swine Tracheal Epithelium. *FEBS Lett.* **1997**, *404*, 192–196.

(45) Mammen, M.; Choi, S. K.; Whitesides, G. M. Polyvalent Interactions in Biological Systems: Implications for Design and Use of Multivalent Ligands and Inhibitors. *Angew. Chem. Int. Ed.* **1998**, *37* (20), 2754–2794.

(46) Dam, T. K.; Roy, R.; Pagé, D.; Brewer, C. F. Negative Cooperativity Associated with Binding of Multivalent Carbohydrates to Lectins. Thermodynamic Analysis of the "Multivalency Effect." *Biochemistry* **2002**, *41* (4), 1351–1358.

Table of Contents:

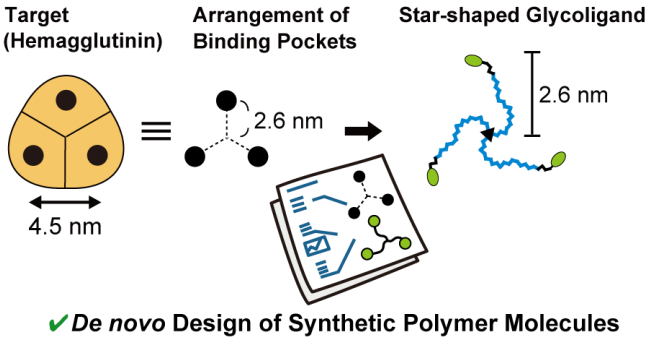

✔*De novo* Design of Synthetic Polymer Molecules